The intrinsic behavior of lithium fluoride in solid electrolyte interphases on lithium

As Published: 10.1073/PNAS.1911017116

Publisher: Proceedings of the National Academy of Sciences

Persistent URL: https://hdl.handle.net/1721.1/136636

Version: Final published version: final published article, as it appeared in a journal, conference proceedings, or other formally published context

The intrinsic behavior of lithium fluoride in solid electrolyte interphases on lithium

Mingfu He[a], Rui Guo[a], Gustavo M. Hobold[a], Haining Gao[b], and Betar M. Gallant[a,1]

[a]Department of Mechanical Engineering, Massachusetts Institute of Technology, Cambridge, MA 02139; and [b]Department of Materials Science and Engineering, Massachusetts Institute of Technology, Cambridge, MA 02139

Edited by Alexis T. Bell, University of California, Berkeley, CA, and approved November 14, 2019 (received for review June 26, 2019)

Lithium is the most attractive anode material for high-energy density rechargeable batteries, but its cycling is plagued by morphological irreversibility and dendrite growth that arise in part from its heterogeneous "native" solid electrolyte interphase (SEI). Enriching the SEI with lithium fluoride (LiF) has recently gained popularity to improve Li cyclability. However, the intrinsic function of LiF—whether chemical, mechanical, or kinetic in nature—remains unknown. Herein, we investigated the stability of LiF in model LiF-enriched SEIs that are either artificially preformed or derived from fluorinated electrolytes, and thus, the effect of the LiF source on Li electrode behavior. We discovered that the mechanical integrity of LiF is easily compromised during plating, making it intrinsically unable to protect Li. The ensuing in situ repair of the interface by electrolyte, either regenerating LiF or forming an extra elastomeric "outer layer," is identified as the more critical determinant of Li electrode performance. Our findings present an updated and dynamic picture of the LiF-enriched SEI and demonstrate the need to carefully consider the combined role of ionic and electrolyte-derived layers in future design strategies.

Li metal anode | Li battery | solid electrolyte interface

Growing demand for electric vehicles has spurred intensive research on rechargeable batteries with higher energy densities than today's Li-ion batteries, which have difficulty meeting energy density targets for transportation (>350 Wh/kg_{cell}) outlined by the US Department of Energy (1). Replacing the graphite anode with Li metal is one potentially promising strategy given a more than 10-fold higher capacity of Li (3,860 mAh/g_{Li} vs. 372 $mAh/g_{graphite}$) (2, 3). Li anodes are also indispensable for realizing the full potential of other "beyond Li-ion" batteries such as Li-oxygen and Li-sulfur (4). However, the use of Li metal faces multiple challenges, especially the propensity to deposit unevenly, leading to dendrite growth, safety issues, and loss of active Li.

Uneven Li deposition is believed to arise in part from the heterogeneity of the Li interface, i.e., the "native" solid electrolyte interphase (SEI), which is made up of multicomponent inorganic and organic phases formed by parasitic reactions between Li and the electrolyte (5, 6). Recently, low Li deposition overpotentials and directional Li^+ migration toward Li nuclei have also been suggested to induce uneven Li deposition (7). Previous research has elucidated certain phenomenological aspects of the SEI, such as the major chemical phases, possible reaction pathways (8), and microscale morphology (9). Lithium fluoride (LiF) is one recurring motif that is present in nearly all functional SEIs (Fig. 1*A*) given fluorine's near ubiquity in common electrolyte salts (10). Among SEI components, bulk LiF possesses some unique properties, including high mechanical strength (11), low solubility (12), a wide electrochemical stability window (0 to 6.4 V vs. Li) (13, 14), and low calculated barriers to Li diffusion (15), which suggests that LiF may enable homogeneous Li^+ flux and suppress dendrites. Consequently, the prevalence of fluorine or fluoride, combined with its attractive properties in the bulk phase, has led to the suggestion that LiF is a particularly beneficial phase for the Li SEI in recent years.

Multiple studies have reported ex situ fabrication of LiF layers on Cu or Li, forming an artificial (also referred to herein as ex situ) LiF SEI (Fig. 1*B*). Synthetic methods have included hydrolysis of $LiPF_6$ on Cu (16, 17); reaction of Li with fluorinated precursors (18, 19); atomic layer deposition (ALD) using TiF_4 (20) or HF/pyridine (21); and physical vapor deposition (22). Smoothened Li deposits were observed after cycling, and several-fold improved cycle life and increased Coulombic efficiencies were generally reported with LiF modification. Other studies have indicated that fluorine or fluoride enrichment in the electrolyte results in a LiF-enriched SEI (herein denoted as "in situ LiF SEI"; Fig. 1*C*). F-enriched electrolytes have included additives such as HF (23) and high loadings of LiF salt (24), and solvents such as fluoroethylene carbonate (FEC) (25–28), and have enabled significant improvements in cycle life and high Coulombic efficiencies (~89 to 99%). High levels of LiF were typically observed in postmortem analysis of the cycled Li surfaces.

Despite these phenomenological improvements, it remains uncertain whether LiF has an intrinsically beneficial function in the SEI. Understanding is hindered by several factors, including variations among LiF-forming approaches (i.e., in situ vs. ex situ) and electrolytes used. For example, conflicting results about ex situ LiF are found in literature: A standalone layer fabricated on Cu by ALD was found to decrease Coulombic efficiency due to inhomogeneous Li deposition (20), whereas LiF layers on Li were elsewhere reported to improve cycle life in symmetric cells (19, 21). Additionally, it remains unclear how some physical properties of LiF can support performance improvements: For example, LiF is an ionic insulator (~10^{-13} to 10^{-14} S/cm) (29, 30), making

Significance

Li metal is one of the most promising anodes for rechargeable batteries due to its large capacity, but its performance is plagued by high chemical reactivity, forming an unstable Li–electrolyte interface. Lithium fluoride has been recently touted as a promising material to improve this interface; however, its intrinsic protective role for Li remains uncertain, hindering design of improved Li interfaces. We demonstrate that the LiF-enriched interface undergoes significant modification as Li^+ ions are cycled through it, and thus that the ensuing solid electrolyte interphase (SEI) repair process from the electrolyte is critical to achieve Li protection.

Author contributions: M.H. and B.M.G. designed research; M.H. and R.G. performed research; R.G., G.M.H., and H.G. contributed new reagents/analytic tools; M.H., H.G., and B.M.G. analyzed data; and M.H. and B.M.G. wrote the paper.

The authors declare no competing interest.

This article is a PNAS Direct Submission.

Data deposition: The analyzed data and metadata reported in this paper have been deposited in the data repository DSpace@MIT, https://hdl.handle.net/1721.1/123103, and are also available upon request to the corresponding author.

[1]To whom correspondence may be addressed. Email: bgallant@mit.edu.

This article contains supporting information online at https://www.pnas.org/lookup/suppl/doi:10.1073/pnas.1911017116/-/DCSupplemental.

First published December 17, 2019.

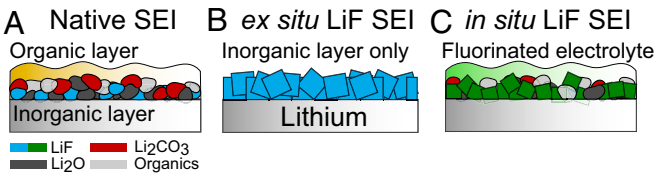

Fig. 1. Varying structures of the LiF-containing solid electrolyte interphase (SEI) on Li. (*A*) Native SEI from conventional carbonate electrolytes, without fluoride enrichment. (*B*) Ex situ LiF-enriched SEI from nonelectrolyte fluorine sources. (*C*) In situ LiF-enriched SEI from fluorine-rich electrolytes.

it counterintuitive that LiF-enriched SEIs can impart benefits related to Li^+ transport.

With these factors in mind, fundamental studies on the intrinsic protective role of LiF are needed. In this work, we aimed to answer the question of whether LiF is a particularly beneficial SEI component from a material point of view. Conformal ex situ LiF layers were first directly grown on Li, and their electrochemical behavior was analyzed in a set of judiciously chosen electrolyte systems to span different SEI-forming functions. This was compared with in situ LiF SEI derived from fluorine-rich electrolytes, providing two platforms to examine the LiF function in detail.

Results and Discussion

Synthesis and Characterization of Ex Situ, All-LiF SEI on Li. To fabricate ex situ layers, a reaction scheme was developed (Fig. 2*A*) to grow LiF directly on Li. Nitrogen trifluoride (NF_3) gas (31) was used as the reactant. We previously studied reduction of NF_3 as a fluorinated gas cathode in Li batteries and found that copious amounts of LiF formed on the carbon cathode under electrochemical conditions, releasing N_2 (32). To develop an analogous chemical synthesis herein, Li foils were mechanically polished under Ar and pressed onto stainless-steel spacers. These were then loaded into a home-built reactor (*SI Appendix*, Fig. S1) and subjected to varying reaction conditions under NF_3 atmosphere at ~20 psi inside an Ar glovebox.

Film composition as a function of reaction condition was first investigated using X-ray photoelectron spectroscopy (XPS). Little reactivity between Li and NF_3 was observed at room temperature (only 1.5% F atomic percentage after 16 h), consistent with the high chemical bond energy of N–F in NF_3 (276 kJ/mol) (33). Increasing the temperature above 150 °C for just 1 h resulted in much higher fluorine content on the Li surface (Fig. 2*B*), corresponding entirely to LiF from the high-resolution F 1s scan (*SI Appendix*, Fig. S2). Negligible elemental nitrogen was observed (<0.3 atomic %; *SI Appendix*, Fig. S2), indicating that N_2 (g) escapes rather than reacting with Li under dry conditions (34). This indicates that the overall synthesis occurs by the reaction 6 Li + 2 NF_3 = 6 LiF + N_2, similar to the electrochemical reaction reported. Notably, the resulting samples had minimal amounts of common contaminant atoms such as C (*SI Appendix*, Fig. S2), which have been present in some other LiF synthetic methods (19, 21). In addition, films formed at 175 °C yielded conformal coverage from scanning electron microscopy (SEM) analysis (Fig. 2*C*; note that air-free sample holders were used to transfer all samples for XPS and SEM measurements). In contrast, only sparse LiF particles were found at lower temperature (150 °C), whereas significantly textured and porous films were observed at higher temperature (190 °C; *SI Appendix*, Fig. S3). At 175 °C, polycrystalline LiF phases were observed from X-ray diffraction (XRD) patterns over a range of reaction times (1 to 15 h), with average grain sizes of 35 to 45 nm (*SI Appendix*, Fig. S4), similar to those of other ex situ LiF layers (10 to 50 nm) (19, 21). A cross-sectional SEM image of an intentionally broken LiF layer after a

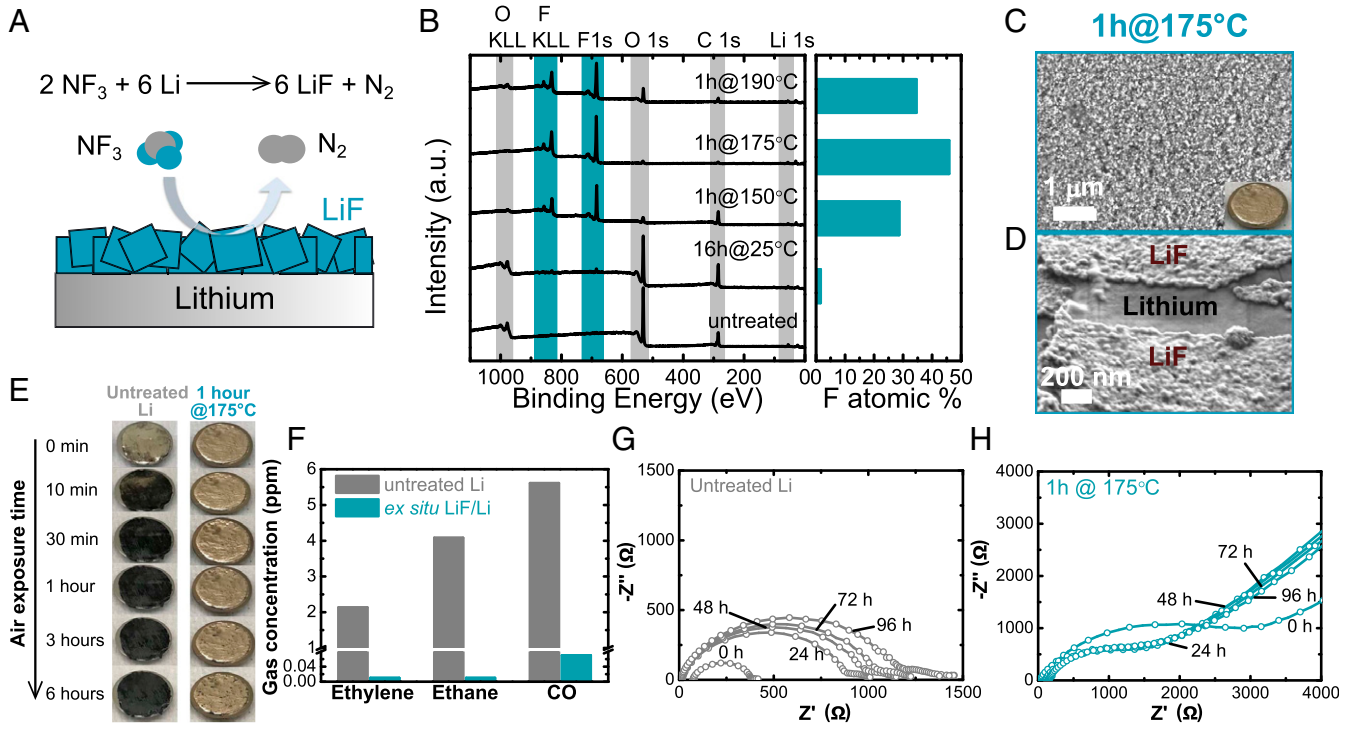

Fig. 2. Synthesis and characterization of ex situ LiF on Li. (*A*) Schematic of the Li–NF_3 reaction to form LiF layers on Li. (*B*) X-ray photoelectron spectra of unreacted and treated Li with corresponding F atomic percentage. (*C*) Top-view and (*D*) tilted-view SEM image, and photograph (*Inset*) of treated Li. The sample in *D* was bent to intentionally break the LiF layer and expose unreacted Li underneath for imaging. (*E*) Photographs of the two types of samples upon air exposure. (*F*) Gas evolution after a 15-min soak of both samples in EC/DEC electrolyte (1 M $LiPF_6$). (*G* and *H*) Nyquist plots of symmetric cells using untreated and treated Li, respectively. Reaction conditions in *C*–*F* and *H* were 175 °C for 1 h.

1-h reaction indicated a thickness of ∼50 nm—similar to other artificially introduced LiF interphases (several to few hundred nanometers) (18, 19, 21, 22) and electrolyte-derived LiF (10)—and that the underlying Li was fully unreacted (Fig. 2*D*). Similar LiF sizes and thicknesses were also obtained at shorter reaction times (5 to 30 min at 175 °C; *SI Appendix*, Fig. S5). This indicates that the growth of LiF particles is self-limited; longer reaction times nucleate more LiF particles but do not cause continuous particle growth. All following measurements utilized films formed at 175 °C for 1 h (denoted henceforth as "ex situ LiF/Li").

Probing the intrinsic stability of an ex situ LiF layer requires that the layer be pinhole-free, i.e., no further reaction occurs between Li and electrolyte when assembled into cells. The as-prepared LiF/Li samples exhibited excellent stability in air over more than 3 h, whereas untreated Li samples reacted readily (Fig. 2*E*). Moreover, upon soaking in excess baseline electrolyte (1 M $LiPF_6$ in ethylene carbonate [EC]: diethylene carbonate [DEC] [vol/vol = 1/1]), untreated Li evolved significant quantities of gases including ethylene (C_2H_4), ethane (C_2H_6), and carbon monoxide (CO) over 15 min, whereas negligible gases were evolved from ex situ LiF/Li (Fig. 2*F*). Furthermore, electrochemical impedance spectroscopy (EIS) measurements were performed at open circuit voltage (OCV) on symmetric cells to examine temporal stability upon soaking (Fig. 2 *G* and *H*). Untreated Li electrodes showed a large depressed semicircle at the high- to medium-frequency region (1 MHz to ∼20 Hz) and a small semicircle-like feature at the low-frequency region (∼20 to ∼1 Hz). The semicircle arises from Li^+ transport through compact ionic phases within the SEI, while the feature at the low-frequency region is associated with Li^+ diffusion at the outermost layer of the SEI; these two features together comprise the Li-electrolyte interfacial resistance (6). Ex situ LiF/Li showed a large semicircle and a straight tail, features that were absent from the pristine Li and can therefore be ascribed to interfacial resistance within the ex situ LiF layer. The real impedances (Z') of the semicircle in the ex situ LiF/Li were significantly larger than those with untreated Li by ∼300 to 700 Ω. Accounting for the thickness of the LiF (∼50 nm) and electrode area (1.33 cm^2), the ionic conductivity of ex situ LiF was estimated as $\sim 10^{-9}$ S/cm, within the range of previously reported ex situ LiF-enriched SEI (10^{-14} to 10^{-9} S/cm) (18, 21). Notably, the impedance results indicate that the ex situ LiF layer is more chemically stable vis-à-vis the electrolyte than a native interface. During the 96-h OCV resting period, the impedance of the former was virtually unchanged, which suggests successful decoupling of the underlying Li from the surrounding electrolyte through a stable LiF film (note that the initial change from 0 to 24 h is due to wetting effects). In contrast, the untreated Li impedance increased steadily over the same time frame, indicating continuous chemical and/or structural evolution of the native SEI (35, 36). These concerted results indicate that the desired model system in Fig. 1*B*—single-component, with minimal solvent-derived outer layer, and representative properties such as thickness, polycrystallinity, and conductivity—was achieved by this synthesis.

Galvanostatic Cycling and Chronoamperometry. We first investigated whether the ex situ LiF SEI retains its pristine structure during active Li plating and stripping. For an ex situ SEI to be deemed fully protective, the layer must enable Li deposition underneath the layer at the Li/SEI interface while avoiding breakage. To investigate whether this occurs with the ex situ LiF SEI, a low current density (0.2 mA/cm^2) was chosen with a cycling capacity of 1 mAh/cm^2. The electrolyte volume was 30 μL. At the onset of cycling (Fig. 3*A*), both ex situ LiF/Li and untreated Li electrodes showed characteristic Li plating behavior, with a relatively large peak voltage followed by a subsequent relaxation (37). However, the LiF/Li electrodes had a significantly larger overpotential than untreated Li, i.e., approximately −600 vs. −320 mV. The higher overpotential in LiF/Li was consistent with the ionic resistance from EIS measurements (∼130 mV for 0.2 mA/cm^2 and ∼500-Ω difference in resistance) and indicates that Li^+ was indeed conducted through the LiF layer during cycling. However, the overpotential difference decreased steadily thereafter, converging to only ∼20 mV within the first full cycle (Fig. 3*B*), suggesting the evolution of the ex situ LiF interface to a less resistive one similar to the native SEI.

Electrode morphologies were analyzed after each sample was subjected to only a single plating/stripping step (Fig. 3 *C* and *D*). In the charged LiF/Li electrode, regions (∼25 μm^2) with darker contrast, corresponding to pitted areas where Li metal was oxidized, were scattered on the electrode surface (Fig. 3*D*, "stripped"). These pitted areas are indicative of SEI breakdown during the electrochemical Li dissolution process as indicated previously (9). Meanwhile, in the corresponding plated electrode, round and whisker-like Li deposits were observed (Fig. 3*D*, "plated"). Notably, these morphological features were nearly indistinguishable from the corresponding untreated Li electrode without LiF (Fig. 3*C*). The increased porosity in the plated ex situ LiF/Li electrode indicates that the LiF layer underwent clear and significant morphological changes, converting into an interface indistinguishable from the untreated Li after only one half-cycle. Thus, LiF does not appear to homogenize Li^+ flux nor enable macroscopic Li deposition beneath the LiF layer. Note that previous studies of ex situ LiF reported SEM images after long-term cycling (e.g., hundreds of cycles)—in some instances, interestingly, with Li deposit morphologies similar to what is reported here—yet were described as being uniform or dendrite-free (22, 38, 39).

We hypothesized that the initially high overpotential and subsequent decrease may be related to the observed breakdown of the initial SEI. To investigate this further, chronoamperometry studies were conducted. Chronoamperometry allows the electrodes to be polarized from the rest state at small incremental potentials, avoiding exposure to potentially damaging high overpotentials. Under these conditions, the ex situ LiF/Li electrode showed significantly smaller current magnitudes (<8 μA/cm^2; Fig. 3*F*) compared to the untreated Li (50 μA/cm^2; Fig. 3*E*), consistent with impeded ion transport through the LiF layer. For untreated Li, current plateaus were rapidly established within several seconds at each step (e.g., −50 μA/cm^2 at −50 mV), indicating that ion transport through the native SEI quickly reached a steady state and that the electrochemically active area remained constant over these short polarization times. Similar current plateaus were also eventually reached with the ex situ LiF/Li electrode at positive potentials. However, monotonic increases in currents after a few seconds (>10 s) were observed at negative potentials below −35 mV. This increasing current magnitude suggests that the electrochemically active area increased after the initial transient period, i.e., SEI breakage occurred, creating a less resistive path for subsequent Li deposition. Thus, the ex situ LiF SEI, by generally impeding ion flux with higher ionic resistance, appears to promote early SEI film breakdown, particularly upon plating. This could occur through enhancements of electrochemical "hot-spot" behaviors (preferred deposition through regions of lower ionic resistance), such as at LiF grain boundaries, which can possibly have enhanced ion transport relative to the bulk as observed in some polycrystalline oxides (40, 41). The fact that the peak overpotential of LiF/Li at the cycling onset (approximately −600 mV, Fig. 3*A*) was significantly larger than the −30 mV at which indications of breakthrough occurred from chronoamperometry indicates that the ex situ LiF SEI is already penetrated at the Li deposition onset under typical galvanostatic conditions. After that, Li plating likely continues through the most preferable path, leading to eventual deposition both within and on top of the LiF layer (Fig. 3*D*).

Compromise of the ex situ LiF SEI during cycling suggests that an SEI-repairing process will occur between the freshly exposed Li and the bulk electrolyte, and that subsequent cycling will be

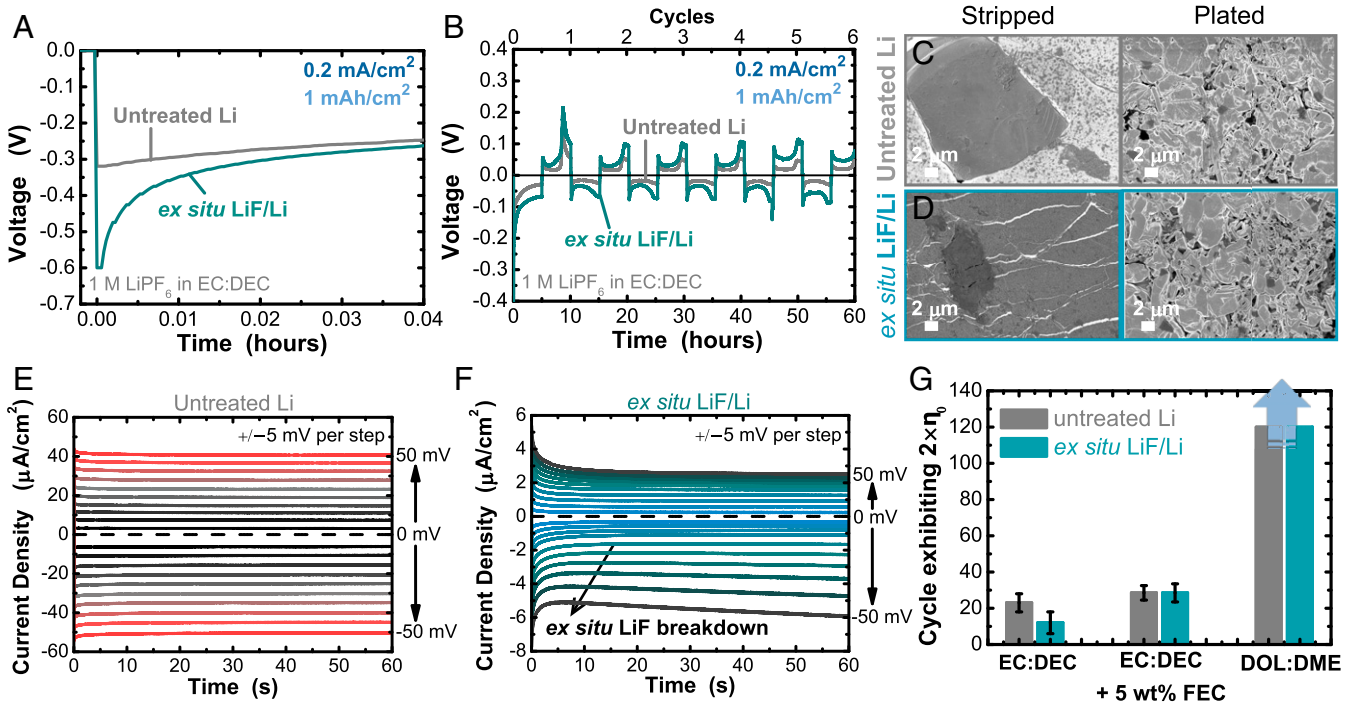

Fig. 3. Cycling of ex situ LiF/Li electrodes. (*A*) Galvanostatic cycling of symmetric Li cells using untreated Li or ex situ LiF/Li during the first half cycle, and (*B*) over the first several cycles. (*C* and *D*) Top-view SEM images of electrodes at the end of the first half-cycle. (*E* and *F*) Chronoamperometry of cells using untreated Li and ex situ LiF/Li as the working electrode, respectively (counter electrode: untreated Li). (*G*) Cell cycle number in which the overpotential doubled compared to the initial reference overpotential (η_0) in different electrolytes. Error bars indicate standard deviation from three cells. The blue arrow indicates user termination of cell cycling after 120 cycles (no differences observed between cells).

electrolyte dependent. To investigate this, electrochemical studies using additional electrolytes—one selected exclusively for "inner-layer" (LiF) repair, and one selected for "outer-layer" (elastomeric) repair—were next conducted. For the first, FEC was added at 5 wt% into the baseline electrolyte because of its reported ability to enrich Li surfaces with LiF (25, 26). To fairly compare cycling outcomes, the cycle number at which the overpotential doubled compared to the initial reference overpotential over the first six cycles was considered (*SI Appendix*, Fig. S6). In the baseline electrolyte, the ex situ LiF/Li had a shorter cycle lifetime before failure compared to the untreated Li, i.e., 12 vs. 23 cycles (Fig. 3*G*). Using ex situ LiF/Li obtained at other conditions (i.e., 5 to 30 min at 175 °C) also failed to significantly achieve better cycle life (*SI Appendix*, Fig. S7). Adding FEC into this electrolyte slightly increased the cycle lifetime for both untreated and ex situ LiF/Li, confirming a minor beneficial role of FEC. However, both types of electrodes exhibited comparable cycle numbers prior to reaching the failure criterion (~25 cycles; *SI Appendix*, Fig. S8 *A* and *B*), indicating that cycle life was determined more by FEC than by the ex situ LiF SEI. Regardless, FEC was not suitable to enable stable, long-term cycling, as cycled electrodes also showed substantial porosity (*SI Appendix*, Fig. S10 *A* and *B*).

Given the inability of FEC in additive quantities to fully repair the ex situ LiF layer under cycling, an ether-based electrolyte, 1 M lithium bis(trifluoromethane)sulfonimide (LiTFSI) in 1,3-dioxolane/1,2-dimethoxyethane (DOL/DME) with 1 wt% $LiNO_3$, was also investigated. This electrolyte composition was selected given the demonstrated ability of DOL/DME to form a flexible and protective outer layer [e.g., polymeric $LiO(CH_2CH_2OCH_2O)_nLi$ from DOL decomposition] (8, 42). In DOL/DME, both electrodes showed significantly larger cycle numbers (>120 cycles; *SI Appendix*, Figs. S8 *C* and *D* and S9) compared to those obtained in carbonate electrolytes. The performance of LiF/Li and untreated Li was indistinguishable, and neither sample exhibited failure over the cycle numbers examined. Despite better cycle performance, the cycled LiF/Li layers with DOL/DME still exhibited significant roughening compared to the pristine state, although deposits were generally smoother (*SI Appendix*, Fig. S10 *C* and *D*) compared to the carbonate electrolyte. Therefore, degradation is at best delayed, but not fully avoidable, even with a substantially improved outer layer. Overall, this leads to the conclusion that the ex situ LiF enrichment appears to be secondary to the much more highly beneficial elastomeric SEI formed in DOL/DME. In other words, a "good" outer layer buffers the degradation of a "bad" inner layer, and even dominates the electrochemical performance. Similar electrolyte dependency of cycle life was also observed when a higher current density (1 mA/cm^2) was used (*SI Appendix*, Fig. S11).

Galvanostatic Cycling with an In Situ, LiF-Enriched SEI Derived from Fluorinated Electrolyte. Given the importance of in situ modification of the SEI by the electrolyte, it is also interesting to interrogate the protective behavior of a LiF-enriched SEI derived from the electrolyte. Thus, 7 M lithium bis(fluorosulfonyl)amide (LiFSI)/FEC was used as a representative all-fluorinated electrolyte that forms copious LiF during Li cycling (28). To form the in situ layer, electrodes were galvanostatically cycled in this electrolyte as a formation step, prior to subsequent characterization. For microstructural analysis of the as-formed in situ SEI, preparation was conducted directly onto a Cu transmission electron microscopy (TEM) grid by cycling in an asymmetric Cu–Li cell using 7 M LiFSI/FEC for 10 cycles, finishing with a charge step that left only the SEI layer behind (*SI Appendix*, Fig. S12*A*). Scanning transmission electron microscopy (STEM) analysis showed that the resulting SEI layer was ~40 nm thick (Fig. 4*A*), similar to the ex situ LiF. However, in contrast to the ex situ layer, which had a single composition (nanocrystalline LiF with no outer layer), the in situ layer was composed of a crystalline

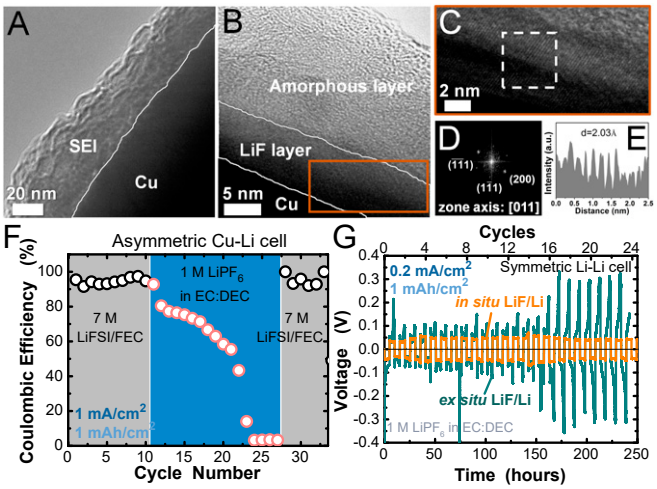

Fig. 4. Characterization and cycling of in situ LiF/Li electrodes. (*A*) Scanning transmission electron microscopy (STEM) image of the in situ LiF SEI formed by plating/stripping Li on a Cu TEM grid. (*B*) Magnified STEM image and (*C*) magnified image of the orange rectangle region in *B*. (*D*) Fast Fourier transformation (FFT) pattern and (*E*) intensity plot of the dashed region in *C*. (*F*) Coulombic efficiency of an asymmetric Cu–Li cell in the electrolyte as indicated. (*G*) Galvanostatic cycling of symmetric Li cells.

inner layer (~8 nm) and an amorphous outer layer (~32 nm; Fig. 4*B*), which likely consists of organic/polymeric species from electrolyte decomposition. The inner layer (Fig. 4*C*) could be assigned along the [011] zone axis of a cubic crystal symmetry (Fig. 4*D*) and had a (200) d-spacing of 2.03 Å (Fig. 4*E*), close to the theoretical value of the LiF (200) plane, 2.01 Å. Coulombic efficiencies during the initial 10 cycles ranged from 91 to 97% (Fig. 4*F* and *SI Appendix*, Fig. S12*B*), in reasonable agreement with previous literature results (~89 to 98% in initial cycles) and higher than those typically attainable in carbonate electrolyte (typically 60 to 80%) (28). To further understand the origin of such high Coulombic efficiencies, and whether they are reflective of a stable solid LiF layer, the fluorinated electrolyte was replaced with the nonfluorinated baseline electrolyte, and cycling continued. The Coulombic efficiency dropped rapidly, from ~90 to ~80%, and continued declining over 10 additional cycles. Surprisingly, the Coulombic efficiency could be nearly restored to >90% when the electrolyte was again replaced by 7 M LiFSI/FEC (Fig. 4*F*). This measurement differed from previous studies (25–28), which always retained the fluorine-rich electrolytes throughout cycling. Therefore, it tests the intrinsic stability of the in situ LiF SEI without the compounding effect of LiF repair once the fluorinated electrolyte is removed. The results indicate that the fluorine-rich electrolyte is essential to achieve high Coulombic efficiencies. Without it, the electrolyte-derived LiF SEI is not intrinsically protective for Li, requiring continuous electrolyte consumption.

To further compare the effect of the in situ and ex situ LiF SEI on Li cycling performance under the same conditions, i.e., coating on Li, in situ LiF/Li electrodes were also prepared by cycling untreated Li in symmetric cells using the 7 M LiFSI/FEC electrolyte for 11 cycles (0.2 mA/cm^2, 1 mA/cm^2; *SI Appendix*, Fig. S13). Then, these modified electrodes were transferred into new symmetric cells reassembled using the baseline electrolyte. Interestingly, upon subsequent cycling, the in situ LiF/Li showed significantly better performance, as indicated by a slower rise in overpotential over 24 cycles compared to the ex situ LiF/Li (Fig. 4*G*). Moreover, the in situ LiF/Li exhibited stable overpotentials over a substantially longer lifetime of 80 cycles (*SI Appendix*, Fig. S14). Lower overpotentials in the in situ LiF/Li likely arise from the lower thickness (~8 nm) of LiF compared to the ex situ LiF (~50 nm). In addition, the better cycle life indicates that the thinner LiF layer may also help to reduce highly localized enhancement of Li^+ transport through lower-resistance pathways (current "hot spots" as mentioned previously), which appears to plague the thicker, ex situ LiF layer. The elasticity provided from the amorphous outer layer can also help to delay the LiF breakdown process, in a similar effect of the elastomeric outer layer from the DOL/DME electrolyte. Taken together, the unique double-layer structure of the in situ LiF SEI can explain the lower overpotentials and improved cycling performance compared to ex situ LiF. Note that, however, porous Li deposits and pitted areas were still observed on cycled in situ LiF/Li electrodes (*SI Appendix*, Fig. S15), indicating the LiF breakdown process still occurred. Interestingly, the cycle life of the in situ LiF layer on Li was also longer than the untreated Li (*SI Appendix*, Fig. S16), despite its low Coulombic efficiency (typically 60 to 80%) in the baseline electrolyte (Fig. 4*F*), indicating that apparently stable Li cycling does not necessarily reflect high Coulombic efficiency when large reservoirs of Li are present.

Discussion on the Intrinsic Protective Behavior of LiF in SEI. Our results show that LiF, whether formed through ex situ or in situ methods, undergoes structural change and breaks down regardless of the electrolyte during cycling. Thus, one of the main attractive properties of bulk LiF—its high mechanical strength—does not translate to high mechanical stability in the SEI. The results also show that LiF does not successfully align Li^+ flux through the interface at a scale required to achieve flawless deposition underneath, at least for SEI layers of ~50 nm in this work. These facts point toward little intrinsically beneficial function of LiF once it is already present as a solid phase in the SEI. The remaining question is why do fluorinated additives yield such high Coulombic efficiencies and good cycle performance? First, while the electrolyte consumption per cycle can be minimized using all-fluorinated electrolytes, continuous electrolyte consumption does occur, as high as 1 to 2% Coulombic inefficiency per cycle. The relatively high Coulombic efficiency reflects the fact that fluorinated electrolyte can quickly passivate new Li deposits with a chemically stable solid phase, and thus

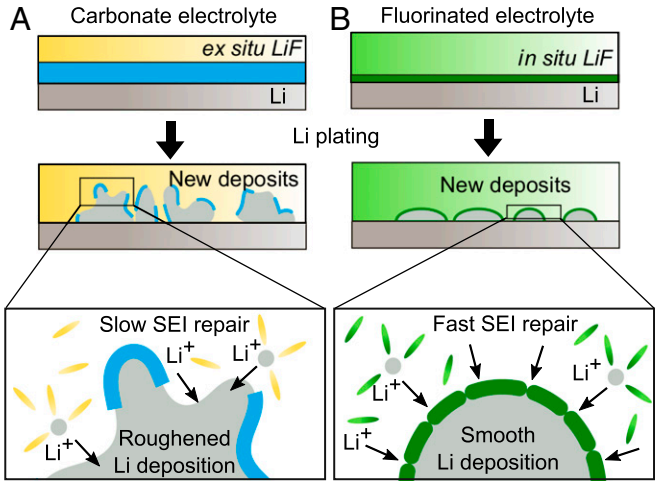

Fig. 5. Li deposition with (*A*) an ex situ LiF SEI in carbonate electrolyte, and (*B*) an in situ LiF SEI in fluorinated electrolyte. Both LiF SEIs break down after Li deposition, but their SEI repair process is kinetically different. Slow repair occurs in the carbonate electrolyte, forming a thick, porous native SEI (*A*), while fluorine sources react quickly with new Li deposits, forming a thin, compact SEI (*B*).

minimize—although not prevent—further reaction of Li with the electrolyte (Fig. 5). Compared to conventional solvents, fluorinated solvents possess lower-energy lowest unoccupied molecular orbitals and thus higher reduction potentials vs. Li (43), which predicts a faster reaction with Li to form a thin and more compact SEI. Fast kinetics of decomposition reactions has been suggested as an important predictor to choose electrolyte components for a stable SEI (44); fluorinated electrolytes embody the concept of a "highly concentrated additive." Future studies that can quantify the kinetics of SEI-forming reactions, particularly those involving fluorinated molecules of different chemical compositions (28), will be important. This kinetics argument also suggests that a "good" SEI may not be unique to LiF-containing compositions, but rather, other species that react rapidly due to elevated potentials vs. Li—which likely explains the success of $LiNO_3$ (45) among other additives. To the best of our knowledge, it has not been mentioned clearly among studies on Li electrodes (46) to date that highly fluorinated electrolytes function by continuous consumption of the electrolyte—in other words, that fluorine enrichment does not create one subsequently stable SEI, such as that observed in the graphite anode (47), but rather is essential for sustained repair of an intrinsically unstable interface.

Conclusions

We have compared the effect of ex situ and in situ LiF-enriched SEIs on Li cycling behavior. The ex situ LiF SEI exhibits breakdown behavior from the cycling onset and fails to intrinsically protect the exposed Li; it is the ensuing Li reaction with the electrolyte, i.e., the in situ SEI formation process, that determines the Li cycling performance. Electrolytes that can form LiF to repair the SEI, or produce an elastomeric outer layer, can substantially improve Li cycling. The in situ LiF SEI also suffers from the same breakdown process and cannot protect new Li deposits once the LiF-forming electrolyte is removed. Thus, our results indicate that the in situ formation of a thin, compact LiF layer to quickly protect the Li surface may be more critical than the properties of LiF itself for affecting Li cycling. They also demonstrate the need to carefully examine the combined role of artificially modified Li alongside possible contributions from the electrolyte, and point to design of electrolytes for fast SEI repair as a promising future strategy in Li battery research.

Materials and Methods

Ex situ LiF/Li electrodes and in situ LiF layer were obtained by reacting polished Li foils with NF_3 gas and cycling electrodes (bare Cu or Li foils) in 7 M LiFSI/FEC electrolyte, respectively. Galvanostatic discharge/charge cycles of symmetric Li–Li or asymmetric Cu–Li cells were carried out on a battery analyzer (model: BST8MA; MTI Corporation). More details on the materials and methods can be found in *SI Appendix*.

ACKNOWLEDGMENTS. The authors gratefully acknowledge support from the National Science Foundation under Award 1804247. M.H. acknowledges financial support from a Massachusetts Institute of Technology (MIT) Bose Fellowship research grant. This work made use of the Materials Research Science and Engineering Center Shared Experimental Facilities at MIT, supported by the National Science Foundation under Award DMR-14-19807.

1. Office of Energy Efficiency and Renewable Energy, US DRIVE electrochemical energy storage roadmap (2017). https://www.energy.gov/eere/vehicles/downloads/us-drive-electrochemical-energy-storage-technical-team-roadmap. Accessed 23 June 2019.
2. D. Lin, Y. Liu, Y. Cui, Reviving the lithium metal anode for high-energy batteries. *Nat. Nanotechnol.* **12**, 194–206 (2017).
3. M. D. Tikekar, S. Choudhury, Z. Tu, L. A. Archer, Design principles for electrolytes and interfaces for stable lithium-metal batteries. *Nat. Energy* **1**, 16114 (2016).
4. P. G. Bruce, S. A. Freunberger, L. J. Hardwick, J.-M. Tarascon, Li-O_2 and Li-S batteries with high energy storage. *Nat. Mater.* **11**, 19–29 (2011).
5. E. Peled, The electrochemical behavior of alkali and alkaline earth metals in nonaqueous battery systems—the solid electrolyte interphase model. *J. Electrochem. Soc.* **126**, 2047–2051 (1979).
6. A. Zaban, E. Zinigrad, D. Aurbach, Impedance spectroscopy of Li electrodes. 4. A general simple model of the Li–solution interphase in polar aprotic systems. *J. Phys. Chem.* **100**, 3089–3101 (1996).
7. D. Rehnlund, C. Ihrfors, J. Maibach, L. Nyholm, Dendrite-free lithium electrode cycling via controlled nucleation in low $LiPF_6$ concentration electrolytes. *Mater. Today* **21**, 1010–1018 (2018).
8. D. Aurbach, E. Zinigrad, Y. Cohen, H. Teller, A short review of failure mechanisms of lithium metal and lithiated graphite anodes in liquid electrolyte solutions. *Solid State Ion.* **148**, 405–416 (2002).
9. Y. S. Cohen, Y. Cohen, D. Aurbach, Micromorphological studies of lithium electrodes in alkyl carbonate solutions using in situ atomic force microscopy. *J. Phys. Chem. B* **104**, 12282–12291 (2000).
10. S. Jurng, Z. L. Brown, J. Kim, B. L. Lucht, Effect of electrolyte on the nanostructure of the solid electrolyte interphase (SEI) and performance of lithium metal anodes. *Energy Environ. Sci.* **11**, 2600–2608 (2018).
11. C. Monroe, J. Newman, The effect of interfacial deformation on electrodeposition kinetics. *J. Electrochem. Soc.* **151**, A880–A886 (2004).
12. J. Jones *et al.*, Thermodynamic of LiF dissolution in alkylcarbonates and some of their mixtures with water. *Fluid Phase Equilib.* **285**, 62–68 (2009).
13. W. D. Richards *et al.*, Interface stability in solid-state batteries. *Chem. Mater.* **28**, 266–273 (2016).
14. Y. Zhu, X. He, Y. Mo, Origin of outstanding stability in the lithium solid electrolyte materials: Insights from thermodynamic analyses based on first-principles calculations. *ACS Appl. Mater. Interfaces* **7**, 23685–23693 (2015).
15. Y. Ozhabes, D. Gunceler, T. A. Arias, Stability and surface diffusion at lithium-electrolyte interphases with connections to dendrite suppression. arXiv:1504.05799 (22 April 2015).
16. X.-Q. Zhang *et al.*, Columnar lithium metal anodes. *Angew. Chem. Int. Ed. Engl.* **56**, 14207–14211 (2017).
17. W. Chang, J. H. Park, D. A. Steingart, Poor man's atomic layer deposition of LiF for additive-free growth of lithium columns. *Nano Lett.* **18**, 7066–7074 (2018).
18. D. Lin *et al.*, Conformal lithium fluoride protection layer on three-dimensional lithium by nonhazardous gaseous reagent freon. *Nano Lett.* **17**, 3731–3737 (2017).
19. J. Zhao *et al.*, Surface fluorination of reactive battery anode materials for enhanced stability. *J. Am. Chem. Soc.* **139**, 11550–11558 (2017).
20. J. Xie, *et al.*, Stitching h-BN by atomic layer deposition of LiF as a stable interface for lithium metal anode. *Sci. Adv.* **3**, eaao3170 (2017).
21. L. Chen *et al.*, Novel ALD chemistry enabled low-temperature synthesis of lithium fluoride coatings for durable lithium anodes. *ACS Appl. Mater. Interfaces* **10**, 26972–26981 (2018).
22. L. Fan *et al.*, Regulating Li deposition at artificial solid electrolyte interphases. *J. Mater. Chem. A* **5**, 3483–3492 (2017).
23. S. Shiraishi, K. Kanamura, Z. Takehara, Surface condition changes in lithium metal deposited in nonaqueous electrolyte containing HF by dissolution-deposition cycles. *J. Electrochem. Soc.* **146**, 1633–1639 (1999).
24. Y. Lu, Z. Tu, L. A. Archer, Stable lithium electrodeposition in liquid and nanoporous solid electrolytes. *Nat. Mater.* **13**, 961–969 (2014).
25. X. Q. Zhang *et al.*, Fluoroethylene carbonate additives to render uniform Li deposits in lithium metal batteries. *Adv. Funct. Mater.* **27**, 1605989 (2017).
26. E. Markevich *et al.*, Very stable lithium metal stripping–plating at a high rate and high areal capacity in fluoroethylene carbonate-based organic electrolyte solution. *ACS Energy Lett.* **2**, 1321–1326 (2017).
27. X. Fan *et al.*, Non-flammable electrolyte enables Li-metal batteries with aggressive cathode chemistries. *Nat. Nanotechnol.* **13**, 715–722 (2018).
28. L. Suo *et al.*, Fluorine-donating electrolytes enable highly reversible 5-V-class Li metal batteries. *Proc. Natl. Acad. Sci. U.S.A.* **115**, 1156–1161 (2018).
29. H. Yildirim, A. Kinaci, M. K. Y. Chan, J. P. Greeley, First-principles analysis of defect thermodynamics and ion transport in inorganic SEI compounds: LiF and NaF. *ACS Appl. Mater. Interfaces* **7**, 18985–18996 (2015).
30. T. G. Stoebe, Influence of OH^- ions on infrared absorption and ionic conductivity in lithium fluoride crystals. *J. Phys. Chem. Solids* **28**, 1375–1382 (1967).
31. B. Golja, J. A. Barkanic, A. Hoff, A review of nitrogen trifluoride for dry etching in microelectronics processing. *Microelectronics J.* **16**, 5–21 (1985).
32. M. He, Y. Li, R. Guo, B. M. Gallant, Electrochemical conversion of nitrogen trifluoride as a gas-to-solid cathode in Li batteries. *J. Phys. Chem. Lett.* **9**, 4700–4706 (2018).
33. J. Berkowitz, J. P. Greene, J. Foropoulos, O. M. Nesković, Bonding and ionization energies of N–F and P–F compounds. *J. Chem. Phys.* **81**, 6166–6175 (1984).
34. M. M. Markowitz, D. A. Boryta, Lithium metal-gas reactions. *J. Chem. Eng. Data* **7**, 586–591 (1962).
35. G. Bieker, M. Winter, P. Bieker, Electrochemical in situ investigations of SEI and dendrite formation on the lithium metal anode. *Phys. Chem. Chem. Phys.* **17**, 8670–8679 (2015).
36. N. Takami, T. Ohsaki, K. Inada, The impedance of lithium electrodes in $LiPF_6$-based electrolytes. *J. Electrochem. Soc.* **139**, 1849–1854 (1992).
37. K. N. Wood *et al.*, Dendrites and pits: Untangling the complex behavior of lithium metal anodes through operando video microscopy. *ACS Cent. Sci.* **2**, 790–801 (2016).
38. J. Lang *et al.*, One-pot solution coating of high quality LiF layer to stabilize Li metal anode. *Energy Storage Mater.* **16**, 85–90 (2019).

39. Y. Yuan *et al*., Regulating Li deposition by constructing LiF-rich host for dendrite-free lithium metal anode. *Energy Storage Mater.* **16**, 411–418 (2019).
40. K. McKenna, A. Shluger, The interaction of oxygen vacancies with grain boundaries in monoclinic HfO_2. *Appl. Phys. Lett.* **95**, 222111 (2009).
41. N. R. Williams, M. Molinari, S. C. Parker, M. T. Storr, Atomistic investigation of the structure and transport properties of tilt grain boundaries of UO_2. *J. Nucl. Mater.* **458**, 45–55 (2015).
42. C. Li, Q. Lan, Y. Yang, H. Shao, H. Zhan, Flexible artificial solid electrolyte interphase formed by 1,3-dioxolane oxidation and polymerization for metallic lithium anodes. *ACS Appl. Mater. Interfaces* **11**, 2479–2489 (2019).
43. T. Achiha *et al*., Thermal stability and electrochemical properties of fluorine compounds as nonflammable solvents for lithium-ion batteries. *J. Electrochem. Soc.* **157**, A707–A712 (2010).
44. E. Peled, D. Golodnitsky, C. Menachem, D. Bar-Tow, An advanced tool for the selection of electrolyte components for rechargeable lithium batteries. *J. Electrochem. Soc.* **145**, 3482–3486 (1998).
45. C. Yan *et al*., Lithium nitrate solvation chemistry in carbonate electrolyte sustains high-voltage lithium metal batteries. *Angew. Chem. Int. Ed. Engl.* **57**, 14055–14059 (2018).
46. R. Jung *et al*., Consumption of fluoroethylene carbonate (FEC) on Si-C composite electrodes for Li-ion batteries. *J. Electrochem. Soc.* **163**, A1705–A1716 (2016).
47. M. Winter, B. Barnett, K. Xu, Before Li ion batteries. *Chem. Rev.* **118**, 11433–11456 (2018).